Supporting Information

Boosting free radical type photocatalysis over Pd/MOFs coordination structure engineering

Hongmei Cheng,[a] Cuicui Zang,[a] Fengxia Bian,[a] Yanke Jiang,*[a] Lin Yang,[a] Fan Dong,[b] Heyan Jiang *[a]

[a] Key Laboratory of Catalysis Science and Technology of Chongqing Education Commission, Chongqing Key Laboratory of Catalysis and New Environmental Materials, College of Environmental and Resources, Chongqing Technology and Business University, Chongqing 400067, China.

[b] Research Center for Environmental and Energy Catalysis, Institute of Fundamental and Frontier Sciences, University of Electronic Science and Technology of China, Chengdu 611731, China.

E-mail: orgjiang@163.com.

1. Materials

All the reagents were commercially available and used without further purification. 1,4-benzenedicarboxylic acid (H_2BDC) and 1,3,5-benzenetricarboxylic acid (H_3BTC) were purchased from Sigma Aldrich. Iron chloride hexahydrate ($FeCl_3 \cdot 6H_2O$), iron (III) nitrate nonahydrate ($Fe(NO_3)_3 \cdot 9H_2O$), N,N-dimethylformamide (DMF), n-hexane, and methanol were supplied by Sinopharm Chemical Reagent Co. Ltd., China.

2. Catalysts preparation

2.1. Preparation of MIL-53(Fe). MIL-53(Fe) was synthesized using a modified method of Férey et al.[S1] A mixture of $FeCl_3 \cdot 6H_2O$ (15 mmol, 4.050 g), H_2BDC (7.5 mmol, 1.236 g) and DMF (45 mL) were subjected to ultrasonic agitation. The resulted homogeneous solution was transferred to a Teflon autoclave and heated at 170 °C for 24 h. The as-obtained powders was isolated by filtration and washed with a large volume of methanol. Finally, the MIL-53(Fe) was harvested after vacuum treatment at 100 °C.

2.2. Preparation of MIL-101(Fe). MIL-101(Fe) was prepared by a reported facile solvothermal method but with some modifications.[S2] Typically, $FeCl_3 \cdot 6H_2O$ (7.5 mmol, 2.025 g) and H_2BDC (3.75 mmol, 0.618 g) were separately dissolved in 30 mL DMF. After sonication to obtain a clear solution, the DMF solution of H_2BDC was added dropwise to the DMF solution of $FeCl_3 \cdot 6H_2O$. The resulting homogeneous solution was heated at 110 °C for 24 h in a Teflon autoclave. The solid was recovered by filtration and washed several times with a large amount of DMF and methanol. The MIL-101(Fe) was collected after the same vacuum treatment as MIL-53(Fe).

2.3. Preparation of MIL-100(Fe). MIL-100(Fe) was prepared following the procedure described in the literature with slight modification.[S3] Typically, $Fe(NO_3)_3 \cdot 9H_2O$ (6 mmol, 2.424 g) and H_3BTC (5 mmol, 1.051 g) were dissolved in deionized water (30 mL). Then, the resulting solution was stirred and transferred to a Teflon autoclave liner, which was sealed and heated at 180 °C for 12 h. After cooling to 30 °C, the obtained solid product was isolated by centrifugation, and stirred separately in ultrapure water and ethanol at 60 °C for 3 h. The light-orange solid product MIL-100(Fe) was obtained following the above vacuum drying.

2.4 Preparation of Pd/Fe-MOFs. Pd/Fe-MOFs was prepared by a double-

solvent impregnation approach combined with a photoreduction process.[S4,S5] For the impregnation, 100 mg activated Fe-MOFs was suspended in 20 mL dry n-hexane and 0.08 mL aqueous solution containing $PdCl_2$ (3.33 mg, 2 wt% Pd) was added drop wise within 15 min under vigorous stirring. After the mixture was stirred for 8 h, the solid was isolated from the supernatant by decanting and dried under vacuum. The as-obtained solid product was then suspended in degassed anhydrous methanol and the mixture was irradiated under visible light for 10 h. The resultant sample was filtered, washed with methanol and dried overnight at 60 °C.

3. Characterizations

X-ray diffraction (XRD) patterns were collected on a D8 Advance X-ray diffractometer (Bruker, Germany) with Cu Kα radiation. The accelerating voltage and the applied current were 40 kV and 40 mA, respectively. Data were recorded at a scanning rate of $0.04°2\theta$ s^{-1} in the 2θ range of 5-80°. The scanning electron microscopy (SEM) and transmission electron microscopy (TEM) were performed on a Hitachi S-4800 and JEOL JEM-2100F, respectively. Fourier transform Infrared (FTIR) spectra were recorded using KBr discs in the range of 4000-500 cm^{-1} on a Bruker Vector 22 FTIR spectrophotometer. X-ray photoelectron spectroscopy (XPS) was measured on UIVAC-PHI 5000 VersaProbe using monochromatized Al Kα X-ray source, in which all of the binding energies were calibrated with reference to the C 1s peak (284.8 eV). UV-Vis diffuse reflectance spectra (DRS) were recorded on a Shimadzu UV-3600 spectrophotometer in the wavelength range of 200-800 nm ($BaSO_4$ was used as reference). Photoluminescence (PL) spectra were obtained using the Hitachi F-7000. The photoelectrochemical measurements were carried out on an electrochemical workstation (CHI730E, Shanghai Chenhua Limited, China) and the electrochemical impedance spectroscopy (EIS) was achieved on Zahner electrochemical workstation (IM6ex, Zahner Scientific Instruments, German), using a standard three-electrode quartz cell with a working electrode, Ag/AgCl used as reference electrode and Pt slice as counter electrode. Fluorine-doped tin oxide (FTO, 7 Ω per square) decorated with catalyst was used as the working electrode. A 0.5 M Na_2SO_4 aqueous solution was served as the electrolyte. A commercial 300 W Xenon lamp (Beijing Newport Co., Ltd) equipped with a 420 nm cutoff filter was employed as a visible light source. Moreover, electrochemical impedance spectroscopy (EIS) was measured with an open-circuit voltage in a frequency range of 10 mHz -100 kHz

with an amplitude of 5 mV.

In situ diffuse reflectance infrared fourier transform (DRIFT) test of CO adsorption was performed under light conditions. After the sample was mixed with KBr, it was activated for 20 min under 110 °C helium purge conditions. Then, at room temperature and visible light radiation, pure CO gas was entered at a flow rate of 20 mL·min^{-1} for 20 min, and the infrared spectrum was recorded every 2 minutes; finally, helium was used to blow away the gaseous CO, and the infrared spectrum was recorded.

4. Photocatalytic reactions

General method A: thiazole C-H arylation with halogenated benzene.

In a 25 mL dry glass reaction tube equipped with a stir bar, bromobenzene (0.25 mmol), thiazole (2.0 equiv, 0.5 mmol), catalyst (20 mg) and K_2CO_3 (3.0 equiv, 0.75 mmol) was mixed in N,N-Dimethylacetamide (DMA, 2mL) solution. The reactor was then sealed with a rubber cap. The reaction was carried out under a 0.75 W cm^{-2} blue LED (460 nm). After 24 hours reaction, the mixture was centrifuged and filtered, liquid phase products were analyzed by Agilent 7820A gas chromatography (GC) with HP-5 column, and the change of reactants and product concentrations was determined. The products were identified by GC-MS (Agilent HP5975), NMR and compared to known compounds. Desired products were obtained with silica gel chromatography (petroleum ether/ethyl acetate 9:1). The solid catalyst was collected by centrifugation and then thoroughly washed with deionized water and ethanol, and the solid was dried at 60 °C under vacuum for the next cycle.

General Procedure B: decarboxylation cross-coupling reaction between cinnamic acid and iodobenzene

In a 25 ml dry glass reaction tube equipped with a stir bar, iodobenzene (0.2 mmol), cinnamic acid (0.4 mmol), catalyst (20 mg) and base (0.6 mmol) were suspended in DMA (2 mL) and the resultant mixture was degassed and saturated with Ar to remove the dissolved O_2 before the reaction. The reaction was carried out with a 0.75 W cm^{-2} blue LED (460 nm). After 24 hours reaction, the mixture was centrifuged and filtered, liquid phase products were analyzed by Agilent 7820A gas chromatography (GC) with HP-5 column, and the change of reactants and product concentrations was determined. The products were identified by GC-MS (Agilent HP5975), NMR and compared to known compounds. Desired products were obtained

with silica gel chromatography (petroleum ether/ethyl acetate 9:1). The solid catalyst was collected by centrifugation and then thoroughly washed with deionized water and ethanol, and the solid was dried at 60 °C under vacuum for the next cycle.

5. Material characterization

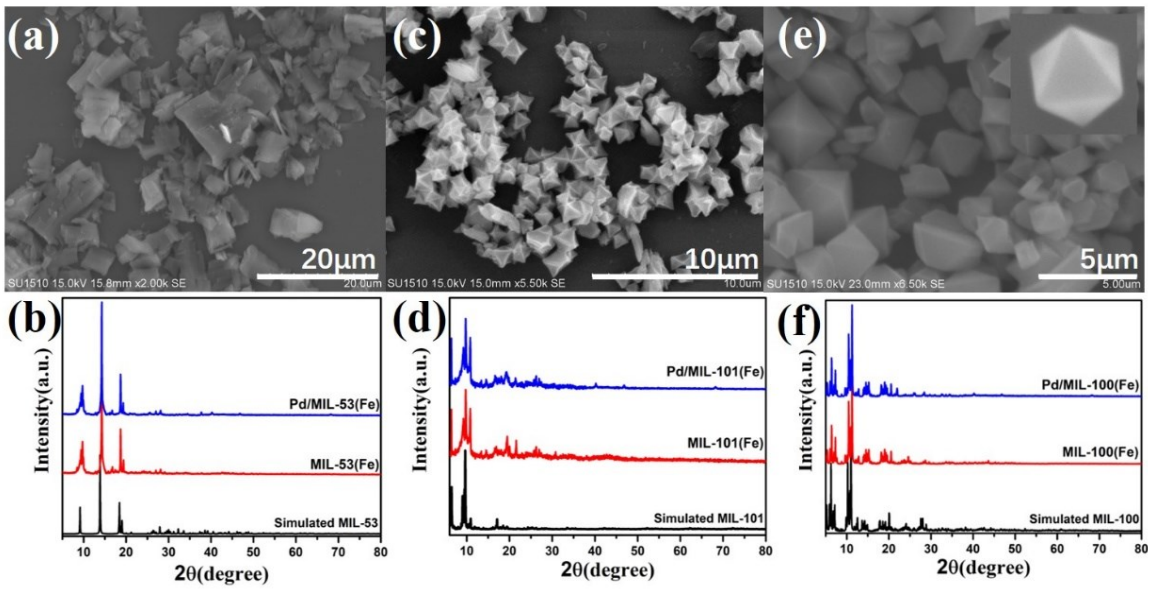

Figure S1. SEM images and XRD patterns of MIL-53(Fe) (a, b); MIL-101(Fe) (c, d); MIL-100(Fe) (e, f).

The SEM images of Fe-MOFs were shown in Figure S1. It is apparent that coordination structure engineered Fe-MOFs were completely different in morphology and particle size. MIL-53(Fe) was composed of irregular lumpy with a size about 5~7 μm (Figure S1a); MIL-101(Fe) exhibited concave octahedron morphology with a uniform particle size of 1.25 μm (Figure S1c); MIL-100(Fe) was composed of octahedral particles with a size approximately 4.62 μm (Figure S1e). The XRD peaks of MIL-53(Fe), MIL-101(Fe) and MIL-100(Fe) in Figure S1 were sharp and well-defined, indicating the high crystallinity. The characteristic peaks were identical with those of previous reports,[S6,S7,S8] suggesting that the target Fe-MOFs were successfully synthesized. The X-ray diffraction patterns of Pd/Fe-MOFs showed three distinct diffraction peaks at 40.1°, 46.6° and 68.1° belong to the characteristic peaks of Pd NPs, corresponding well to the (111), (200) and (220) planes of face-centered cubic (fcc) Pd (PDF#46-1043), respectively.

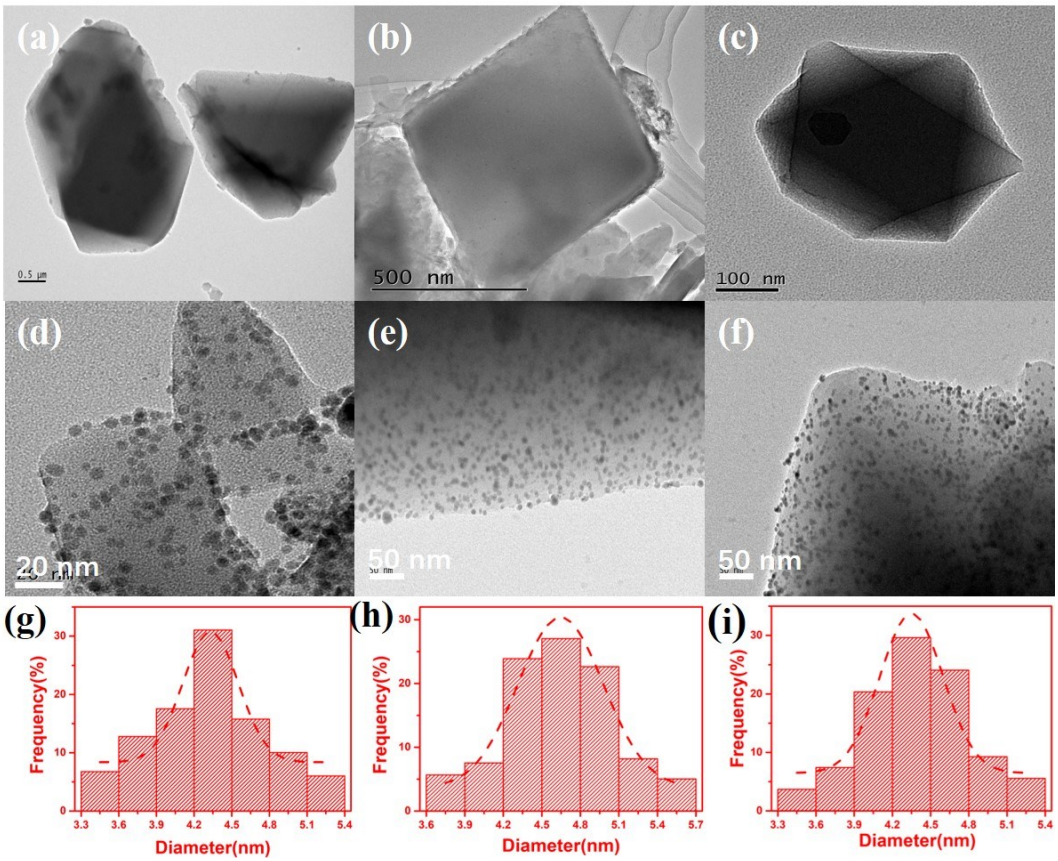

Figure S2. TEM images and Pd NPs size distribution histogram of Pd/MIL-53(Fe) (a, d, g); Pd/MIL-101(Fe) (b, e, h); Pd/MIL-100(Fe) (c, f, i).

The TEM images of Pd/Fe-MOFs and the size distribution of Pd NPs are shown in Figure S2. After photoreduction, Pd NPs were uniformly distributed in MIL-53(Fe), MIL-101(Fe) and MIL-100(Fe), and the average particle sizes were 4.30 nm, 4.7 nm and 4.38 nm, respectively. The average particle sizes of Pd NPs on different Fe-MOFs were basically similar. Compared with the original Fe-MOFs, Fe-MOFs retained the original morphology after Pd NPs loading.

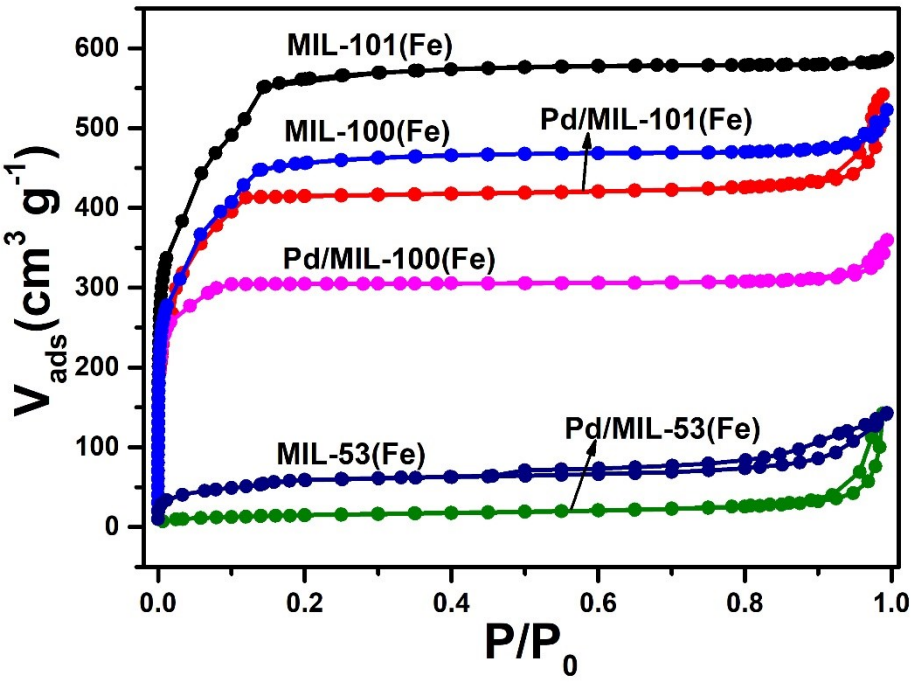

Figure S3. N_2 sorption isotherms of Fe-MOFs and Pd/Fe-MOFs at 77 K.

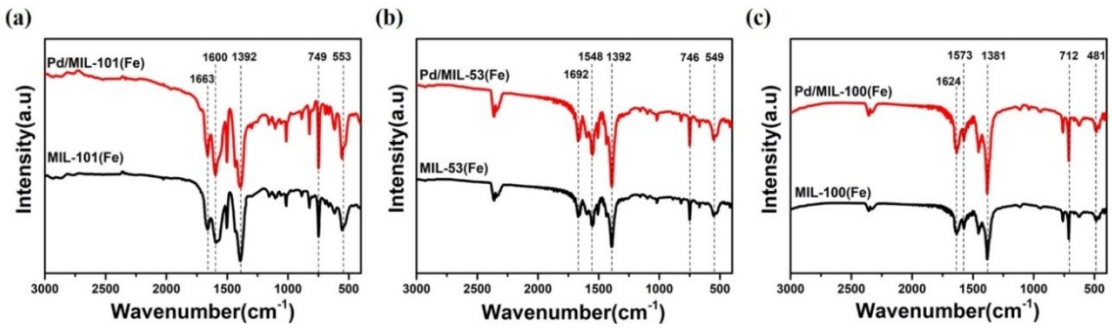

Figure S4. FT-IR spectra of Fe-MOFs and Pd/Fe-MOFs.

The molecular structure and functional group of the coordination structure engineered Fe-MOFs and Pd/Fe-MOFs were characterized by the FT-IR spectroscopy (Figure S4). The feature peaks at 1663, 1600, 1392, 749 and 553 cm^{-1} in the MIL-101(Fe) spectra should be ascribed to the C=O stretching vibration, C=O asymmetric vibration, C=O symmetric vibration, C-H bending vibration in the benzene and stretching vibration of Fe-O, respectively.[S9,S10] Identical to the previous reports, these peaks suggested the presence of dicarboxylate linker and the formation of iron-oxo clusters. The characteristic peaks of MIL-53(Fe) were at 1692, 1548, 1392, 746 and 545 cm^{-1} respectively, and these results proved that MIL-53(Fe) was successfully prepared.[S11] In comparison with MIL-101(Fe), the difference in peak position should be caused by the difference in Fe coordination mode. Additionally, the corresponding peaks in the MIL-100(Fe) FT-IR spectrum were shifted to 1627, 1576, 1381, 712 and 483 cm^{-1}, respectively.[S12] The difference in the peak position should be ascribed to the different organic linker coordinated with Fe (H_3BTC for MIL-100(Fe), H_2BDC for MIL-101(Fe) and MIL-53(Fe). The Fe-MOFs structure crystal integrity maintenance during Pd NPs loading was also confirmed by the Pd/Fe-MOFs FT-IR spectrum.

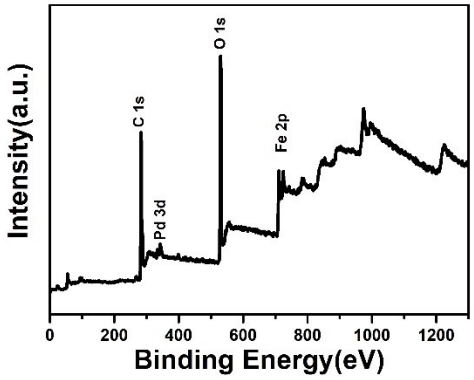

Figure S5. XPS survey spectra of Pd/MIL-101(Fe).

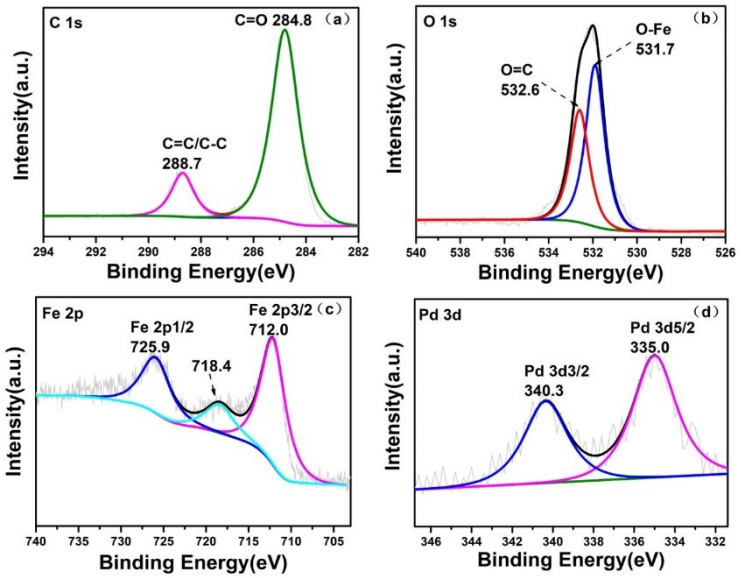

Figure S6. XPS spectra of Pd/MIL-101(Fe): (a) C 1s, (b) O 1s, (c) Fe 2p, and (d) Pd 3d.

The full XPS survey spectra in the range of 0-1350 eV was shown in Figure S5, which verified the existence of Fe, O, C and Pd elements in Pd/MIL-101(Fe). The high-resolution XPS spectrum of C 1s (Figure S6a) had two clearly deconvoluted peaks locating at 284.8 and 288.7 eV, which should be assigned to C=C/C-C and C=O groups of the organic linker in MIL-101(Fe).[S10] The O 1 s spectra (Figure S6b) could be fitted into two peaks locating at 532.6 and 531.7 eV. The two peaks are individually attributed to the O=C component of the organic linker and O-Fe component in Fe-oxo clusters.[S10] As for Fe 2p spectra (Figure S6c), two peaks located at 725.9 and 712.0 eV were assigned to the Fe 2p1/2 and Fe 2p3/2, respectively.[S13] The distance between these two peaks is about 13.9 eV, which agreed well with the typical features of α-Fe_2O_3.[S14] Moreover, the satellite peak at 718.4 eV should be owing to Fe(III). XPS results also confirmed the existence of visible light reduced Pd^0 in Pd/MIL-101(Fe) by showing two peaks at 335.0 and 340.3 eV, corresponding to Pd 3d5/2 and Pd 3d3/2, respectively (Figure S6d). [S5]

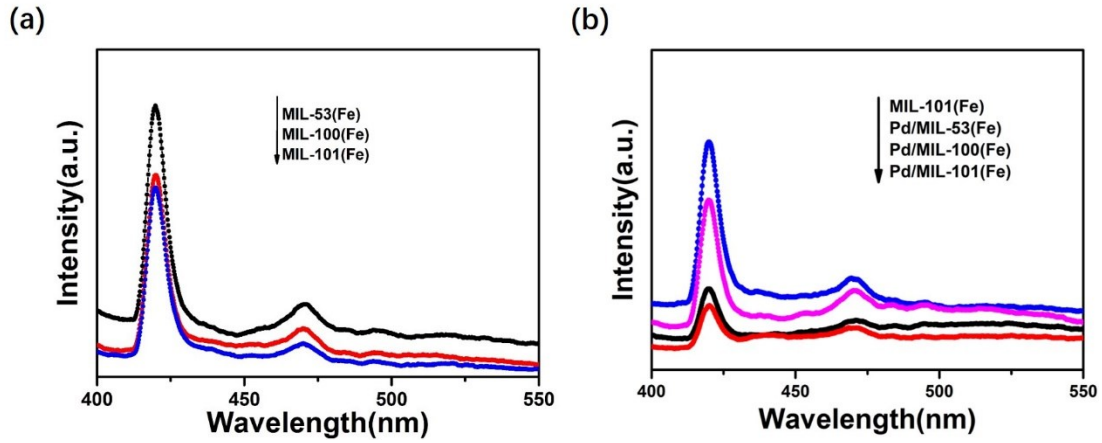

Figure S7. PL spectra of Fe-MOFs and Pd/ Fe-MOFs under 360 nm excitation at room temperature.

PL spectroscopy was used to study the separation and recombination rate of photogenerated electrons and holes in the samples. Figure S7 showed the PL emission spectra of these samples excited at 360 nm. The PL intensity of Pd/MIL-101(Fe) was significantly lower than that of pure MIL-101(Fe), indicating that the introduction of Pd NPs would greatly inhibit the recombination of photogenerated electron-hole pairs in MIL-101(Fe), so there were more electron-hole pairs in Pd/MIL-101(Fe) materials. When comparing Pd/MIL-53(Fe) and Pd/MIL-100(Fe), it was found that different topological structure, various linkers and introduction of metal clusters all had effect on the recombination of photogenerated electron-hole pairs of the catalyst.

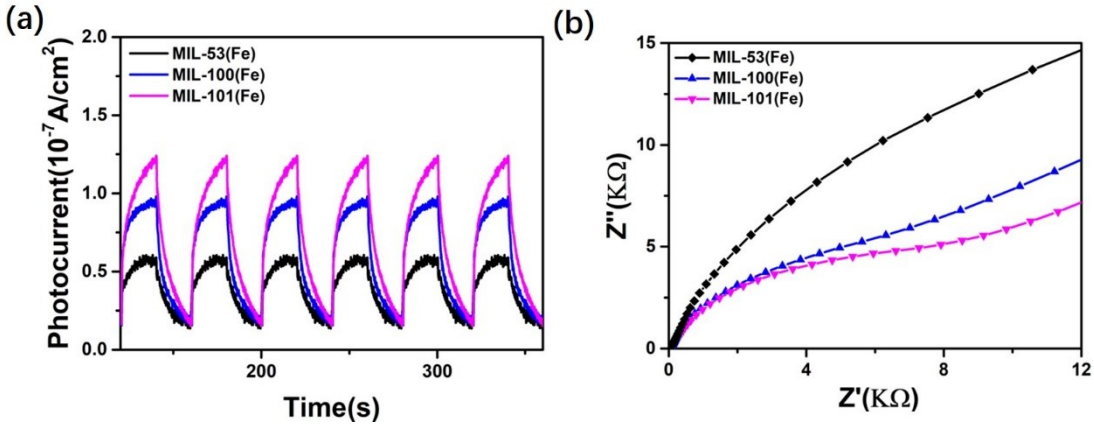

Figure S8. Transient photocurrents recorded under visible light irradiation (a) and EIS Nyquist plots (b) of MIL-101(Fe), MIL-53(Fe) as well as MIL-100(Fe).

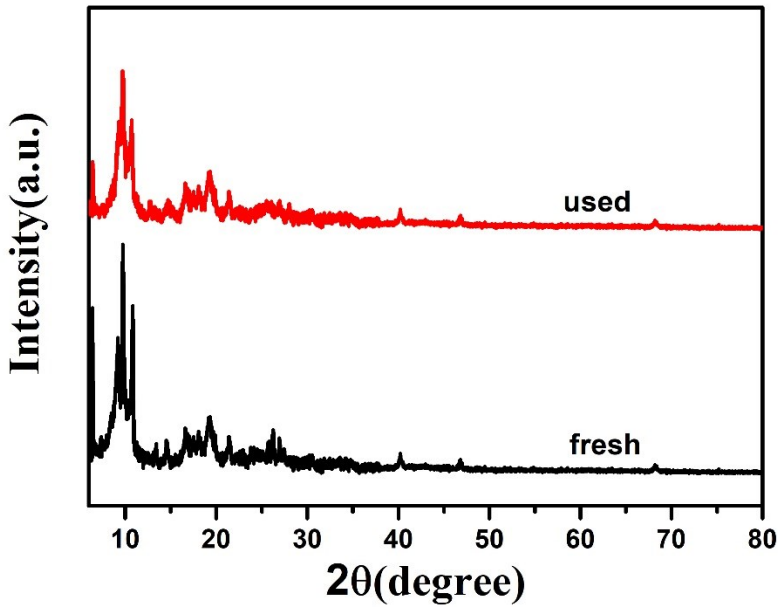

Figure S9. The XRD patterns of fresh and used Pd/MIL-101(Fe).

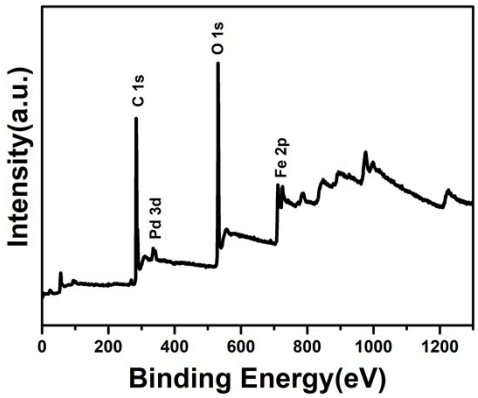

Figure S10. XPS survey spectra of used Pd/MIL-101(Fe).

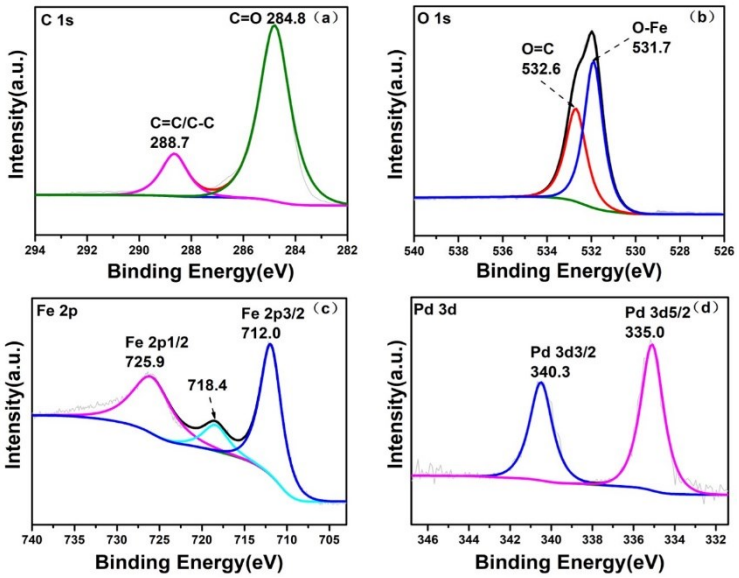

Figure S11. XPS spectra of used Pd/MIL-101(Fe): (a) C 1s, (b) O 1s, (c) Fe 2p, and (d) Pd 3d.

Table S1. BET surface area and pore volume of the MOFs.

Sample	S_{BET} (m^2 g^{-1})	Pore volume (cm^3 g^{-1})
MIL-101(Fe)	2018.9	1.14
Pd/MIL-101(Fe)	1312.6	0.68
MIL-53(Fe)	215.5	0.20
Pd/MIL-53(Fe)	52.6	0.09
MIL-100(Fe)	1632.4	0.76
Pd/MIL-100(Fe)	861.8	0.39

6. Substrate expansion

Table S2. Photocatalytic thiazole C-H arylation under different conditions.

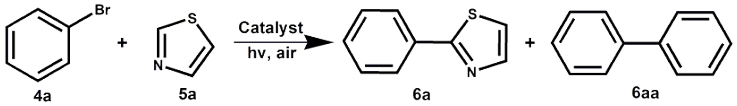

4a 5a 6a 6aa

Entry	Catalyst	Atmosphere	4a Conv. /%	6a Sel. /%
1	2 wt% Pd/MIL-101(Fe)	air	93.1	98.3
2	2 wt% Pd/MIL-101(Fe)	Ar	92.5	98.1
3	2 wt% Pd/MIL-101(Fe)	N_2	92.8	98.5
4	Pd/C	air	17.5	21.7
5	Pd-PVP[S15]	air	15.1	24.1

Reaction conditions unless otherwise noted: 4a (0.25 mmol), 5a (2.0 equiv.), DMA (2.0 mL), catalyst (4 μmol based on Pd), K_2CO_3 (3.0 equiv.), 0.75 W cm^{-2} blue LED (460 nm), irradiated for 24 h.

Table S3. Effect of different Pd loading on the photocatalytic thiazole C-H arylation.

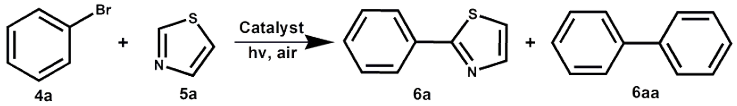

4a 5a 6a 6aa

Entry	Catalyst	4a Conv. /%	6a Sel. /%	TOF(h^{-1})
1	1.5 wt% Pd/MIL-101(Fe)	47.0	99.6	3.3
2	2.0 wt% Pd/MIL-101(Fe)	50.2	99.4	3.5
3	2.5 wt% Pd/MIL-101(Fe)	49.5	99.5	3.4
4	3.0 wt% Pd/MIL-101(Fe)	45.1	99.6	3.1

Reaction conditions unless otherwise noted: 4a (0.25 mmol), 5a (2.0 equiv.), DMA (2.0 mL), catalyst (4 μmol based on Pd), K_2CO_3 (3.0 equiv.), air, 0.75 W cm^{-2} blue LED (460 nm), irradiated for 9 h.

Table S4. Substrate scope of photocatalytic C-H arylation reaction over Pd/ MIL-101(Fe).

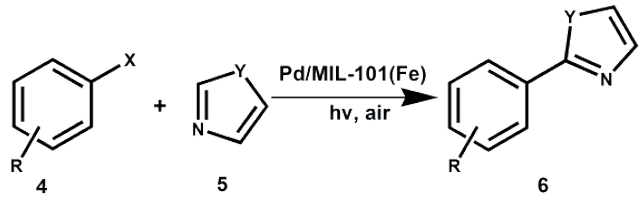

4 5 6

Entry	R	X	Y	4 Conv. /%	6 Sel. /%
1	H	Br	S	93.1	98.3
2	*p*-OMe	Br	S	96.4	99.7
3	*o*-OMe	Br	S	69.9	97.1
4	*p*-CHO	Br	S	65.5	99.8
5	*p*-CF_3	Br	S	40.9	96.2
6	*p*-Me	I	S	96.1	97.1
7	*m*-Me	I	S	93.6	98.9
8	*p*-OMe	I	S	98.9	95.4
9	*m*-OMe	I	S	85.4	99.4
10	*p*-CN	I	S	61.7	94.3
11	*p*-NO_2	I	S	64.0	96.0
12	H	Br	N-CH_3	70.7	97.9

Reaction conditions unless otherwise noted: 4 (0.25 mmol), 5 (2.0 equiv.), DMA (2.0 mL), Pd/MIL-101(Fe) (20 mg, 2 wt% Pd), K_2CO_3 (3.0 equiv.), air, 0.75 W cm^{-2} blue LED (460 nm), irradiated for 24 h.

Table S5. Photocatalytic cinnamic acid decarboxylation cross-coupling reaction under different atmosphere.

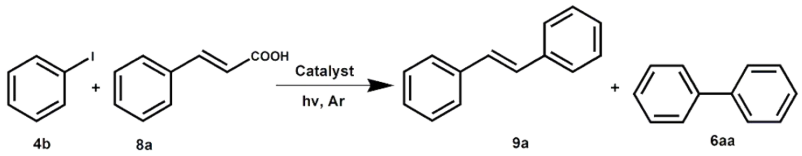

Entry	Catalyst	Atmosphere	4b Conv. /%	9a Sel. /%	E/Z
1	Pd/MIL-101(Fe)	air	93.7	91.2	95/5
2	Pd/MIL-101(Fe)	Ar	94.7	94.2	99/1
3	Pd/MIL-101(Fe)	N_2	95.0	94.1	98/2

Reaction conditions unless otherwise noted: 4b (0.25 mmol), 8a (2.0 equiv.), DMA (2.0 mL), Pd/MIL-101(Fe) (20 mg, 2 wt% Pd), K_2HPO_4 (3.0 equiv.), 0.75 W cm^{-2} blue LED (460 nm), irradiated for 24 h.

There has no obvious catalytic activity difference under various atmosphere, and the best chemoselectivity and stereoselectivity was achieved under Ar.

Table S6. Aryl radical capture with TEPMO over different catalysts.

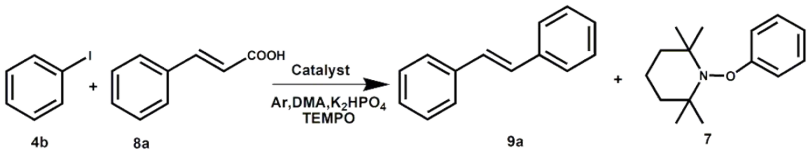

Entry	**Catalyst**	**4b Conv. /%**	**7 Sel. /%**
1	Pd/MIL-101(Fe)	85.4	97.2
2	Pd/MIL-100(Fe)	83.9	96.3
3	Pd/MIL-53(Fe)	60.6	55.6

Reaction conditions unless otherwise noted: 4b (0.25 mmol), 8a (2.0 equiv.), DMA (2.0 mL), catalyst (20 mg, 2 wt% Pd), K_2HPO_4 (3.0 equiv.), TEMPO (4 equiv.), air, 0.75 W cm^{-2} blue LED (460 nm), irradiated for 24 h.

Table S7. Pd/MIL-101(Fe) catalyzed decarboxylative cross-coupling: aryl iodide scope.

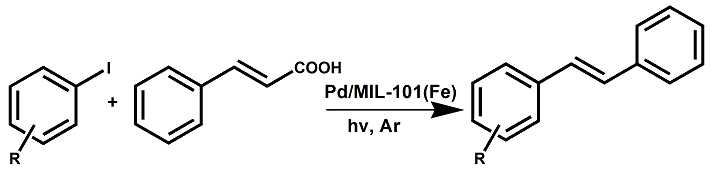

4 8a 9

Entry	R	4 Conv. /%	9 Sel. /%	E/Z
1	H	94.7(90.9)[a]	94.2(74.5)[a]	99/1(14/86)[a]
2	*p*-NH_2	97.2(90.3)	99.0(89.8)	98/2(8/92)
3	*p*-OMe	96.1(79.6)	98.2(80.8)	96/4(6/94)
4	*m*-OMe	70.9(56.7)	97.9(79.9)	99/1(22/78)
5	*o*-OMe	53.5(40.8)	99.7(90.6)	>99/1(30/70)
6	*p*-Me	97.8(88.8)	95.0(88.9)	95/5(7/93)
7	*m*-Me	88.1(79.1)	98.5(73.7)	98/2(25/75)
8	*p*-CN	69.8(61.8)	95.7(79.7)	93/7(3/97)
9	*p*-CF_3	57.5(51.1)	97.8(83.9)	94/6(1/99)
10	*p*-NO_2	61.9(55.3)	95.7(86.3)	99/1(2/98)

Reaction conditions unless otherwise noted: 4 (0.25 mmol), 8a (2.0 equiv.), DMA (2.0 mL), Pd/MIL-101(Fe) (20 mg, 2 wt% Pd), K_2HPO_4 (3.0 equiv.), Ar, 0.75 W cm^{-2} blue LED (460 nm), irradiated for 24 h.

[a] The conversion and E/Z ratio were displayed in brackets when K_2CO_3 was used as the base.

Table S8. Other decarboxylation cross-coupling reactions catalyzed by Pd/MIL-101(Fe).

Entry	4	8	9	4 Conv. /%	9 Sel. /%	E/Z
1	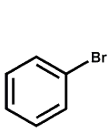	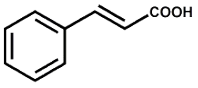	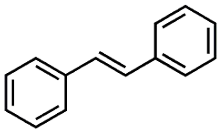	58.5	98.5	>99/1
2	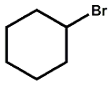	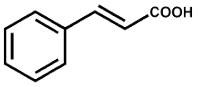	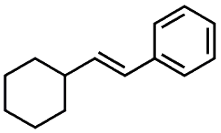	75.5	99.0	>99/1
3	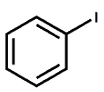	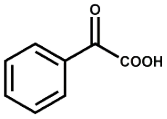	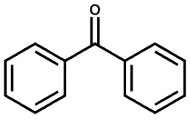	89.8	93.1	

Reaction conditions unless otherwise noted: 4 (0.25 mmol), 8 (2.0 equiv.), DMA (2.0 mL), Pd/MIL-101(Fe) (20 mg), K_2HPO_4 (3.0 equiv.), Ar, 0.75 W cm^{-2} blue LED (460 nm), irradiated for 24 h.

Scheme S1: Scale up experiment: (a) C-H arylation; (b) Decarboxylation cross-coupling reaction

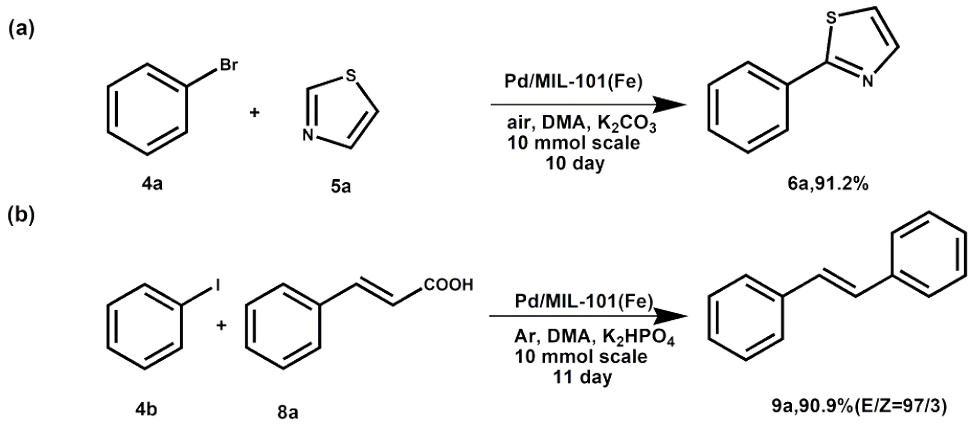

Scale-up experiments were carried out according to procedure A or B. The substrates were expanded 50 times, the amount of catalyst was expanded 5 times, and the reaction time was extended.

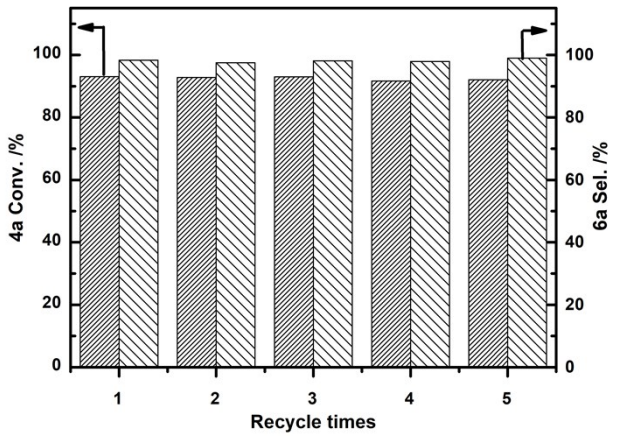

Figure S12. Pd/MIL-101(Fe) recycles for the C-H arylation of bromobenzene (**4a**) with thiazole under visible light irradiation.

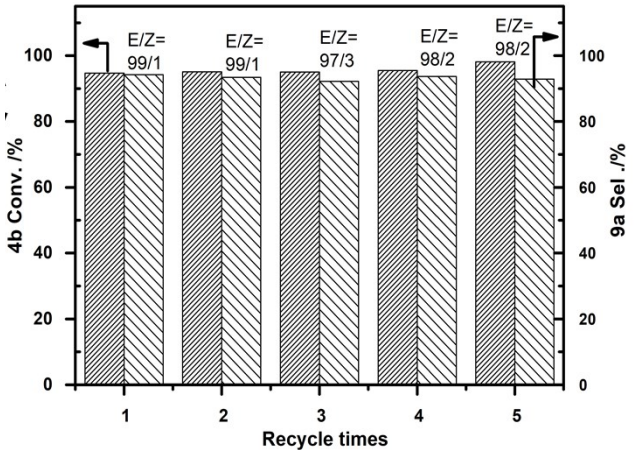

Figure S13. Pd/MIL-101(Fe) recycles for the decarboxylation cross-coupling of iodobenzene (**4b**) with cinnamic acid under visible light irradiation.

7. Mechanism study

7.1 Light on-off experiment

(1) Scheme S2: C-H arylation

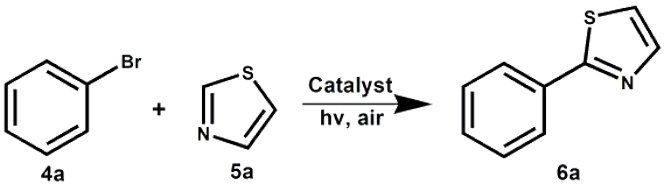

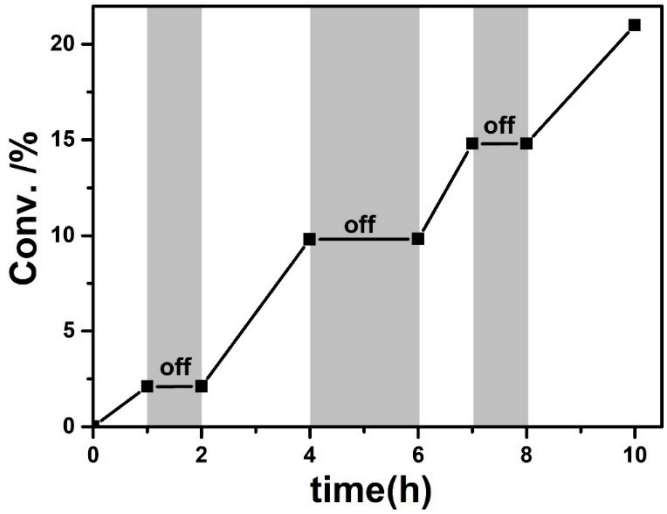

(2) Scheme S3: Decarboxylation cross-coupling reaction

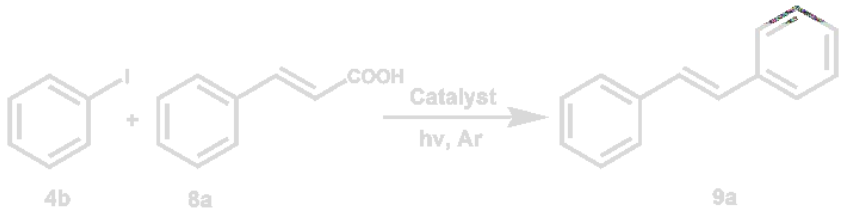

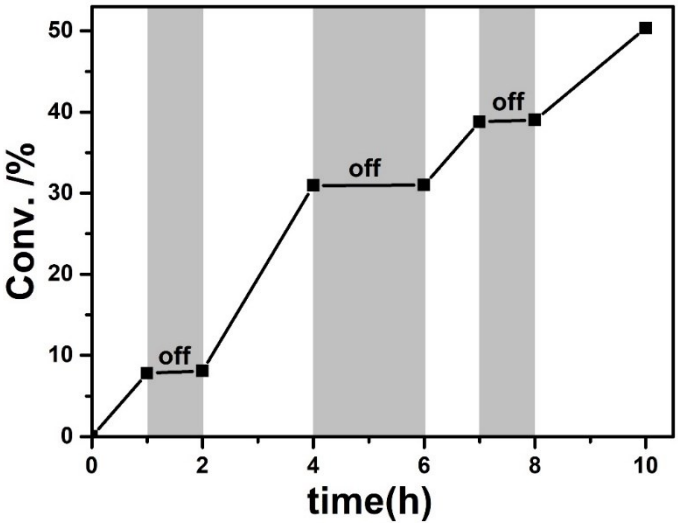

To exclude the possibility of a radical chain process in the reaction, light on-off experiments were carried following the **procedure A** or **procedure B**. The light was kept off during the off-periods and the conversion was determined by GC analysis. No further reaction was observed during the light off-periods, which confirmed that the reactions were not preceded with radical chain propagation mechanism and visible light was a necessary factor for inducing the reactions.

7.2 Control experiment

(1) Scheme S4: Carboxylate anion verification experiment

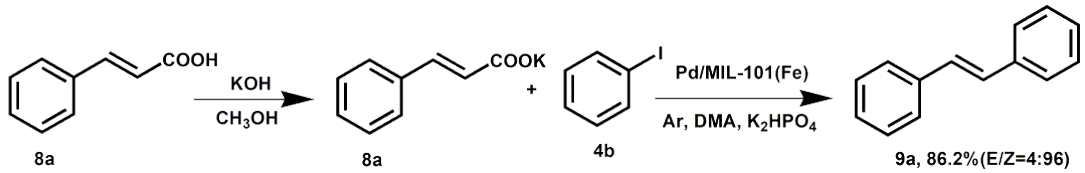

In a 25 ml dry glass reaction tube equipped with a stir bar, dissolve cinnamic acid (0.4 mmol) and KOH (0.4 mmol) in methanol (10 mL), stir for 1 h in the greenhouse, and spin-evaporate to obtain potassium cinnamate. Then, iodobenzene (0.2 mmol), potassium cinnamate, Pd/MIL-101(Fe) (20 mg), and K_2HPO_4 (0.6 mmol) were suspended in DMA (2 mL), the resultant mixture was degassed and saturated with Ar to remove the dissolved O_2 before the reaction. The reaction was carried out under a 0.75 W cm^{-2} blue LED (460 nm). After 24 h of reaction, the mixture was centrifuged and filtered, the product was analyzed by GC and GC-MS equipped with HP-5 capillary column.

(2) Scheme S5: Radical verification experiment

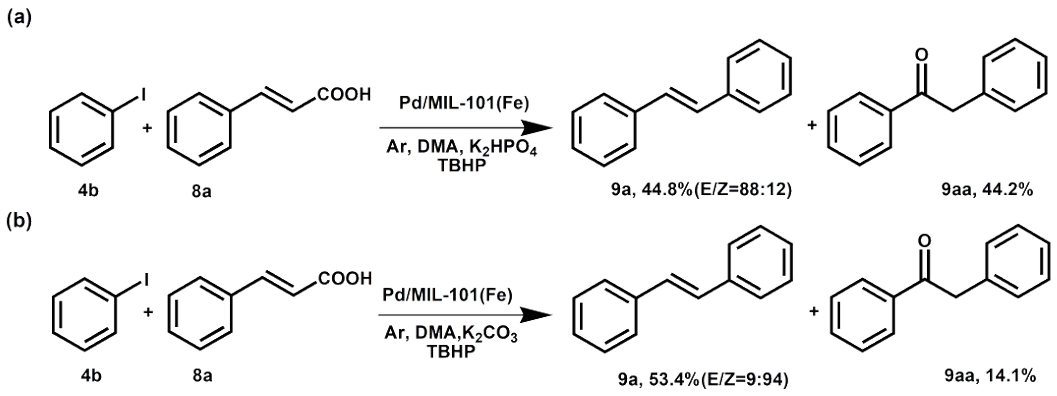

In a 25 ml dry glass reaction tube equipped with a stir bar, iodobenzene (0.2 mmol), cinnamic acid (0.4 mmol), Pd/MIL-101(Fe) (20 mg), K_2HPO_4 or K_2CO_3 (0.6 mmol) and TBHP (0.4 mmol) were suspended in DMA (2 mL), the resultant mixture was degassed and saturated with Ar to remove the dissolved O_2 before the reaction. The reaction was carried out under a 0.75 W cm^{-2} blue LED (460 nm). After 24 h of reaction, the mixture was centrifuged and filtered, the product was analyzed by GC and GC-MS equipped with HP-5 capillary column. Product **9aa** was clearly detected in the reaction mixture with GC-MS.

(3) Scheme S6: Radical mechanism

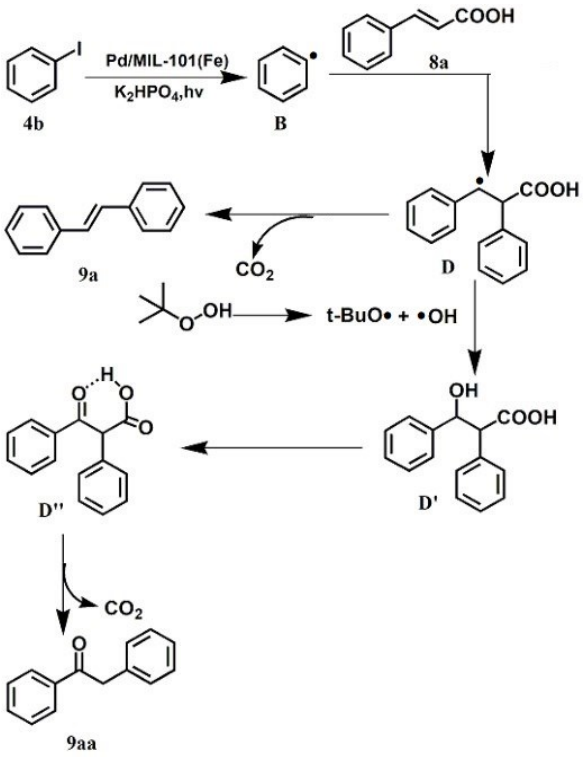

Under the visible light irradiation, iodobenzene was activated to form aryl radical **B**, which was subsequently formed intermediate **D** with cinnamic acid **8a**. The intermediate product **D** formed **9a** through the CO_2 removal over the oxidation of holes. Sun et al.[S16] has demonstrated that the cinnamic acid (**8a**) decarboxylation reaction generated ketones through a free radical mechanism in the presence of Di-tert-butyl peroxide (DTBP) or tert-butyl hydroperoxide (TBHP). According to this experimental method, we designed experiment to clarify the existence of intermediate product **D** in the photocatalytic decarboxylation cross-coupling reaction over Pd/MIL-101(Fe). The combination between radical intermediate **D** and TBHP generated hydroxyl radical would afford the intermediate **D'**, which could be further converted

to α-carbonyl acid intermediate **D"** under oxidative conditions. Finally, thermal decarboxylation would give another desired product **9aa** accompany with CO_2 release. Product **9aa** was clearly detected in the reaction mixture in the presence of TBHP and K_2HPO_4 with GC-MS, therefore, the existence of intermediate product **D** was proved.

8. Reaction Products Characterization

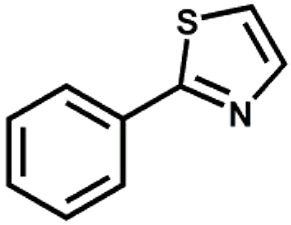

2-Phenylthiazole： ^{1}H NMR (600 MHz, $CDCl_3$) δ 7.31 (d, J = 3.0 Hz, 1H) 7.39-7.46 (m, 3H), 7.85 (d, J = 3.3 Hz, 1H), 7.95-7.97 (m, 2H). MS calculated for C_9H_7NS: 161, found: 161.

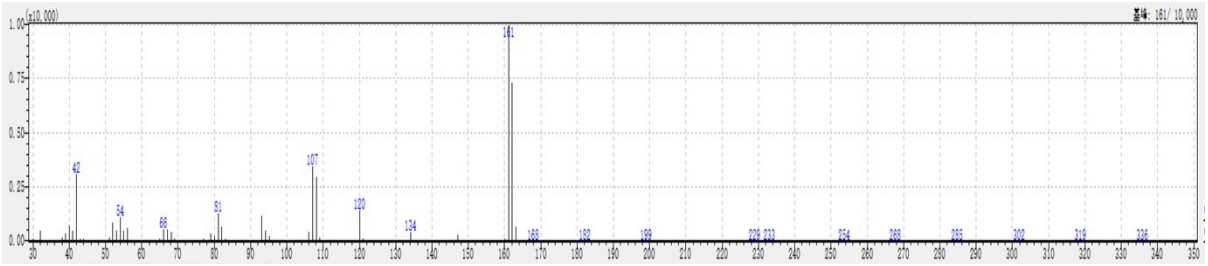

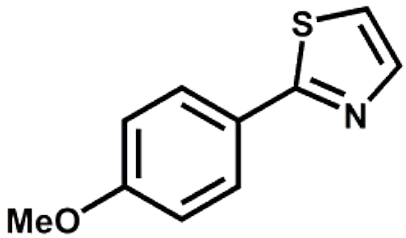

2-(4-methoxyphenyl)thiazole: ^{1}H NMR (600 MHz, $CDCl_3$) δ 3.83 (s, 3H), 6.94 (m, 2H), 7.23 (d, J = 3.5 Hz, 1H), 7.79 (d, J = 3.5 Hz, 1H), 7.89 (m, 2H). MS calculated for $C_{10}H_9NOS$: 191, found: 191.

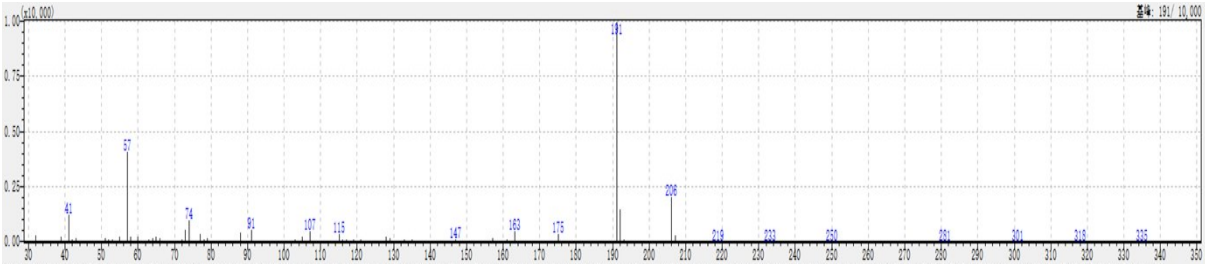

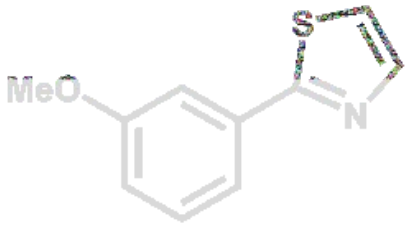

2-(3-methoxyphenyl)thiazole: ^{1}H NMR (600 MHz, $CDCl_3$) δ 3.86 (s, 3H), 6.96 (m, 1 H), 7.30 (d, *J* = 3.3 Hz, 1H), 7.51 (m, 1 H), 7.33 (m, 1H), 7.55 (m, 1H), 7.85 (d, *J* = 3.3 Hz, 1H); MS calculated for $C_{10}H_9NOS$: 191, found: 191.

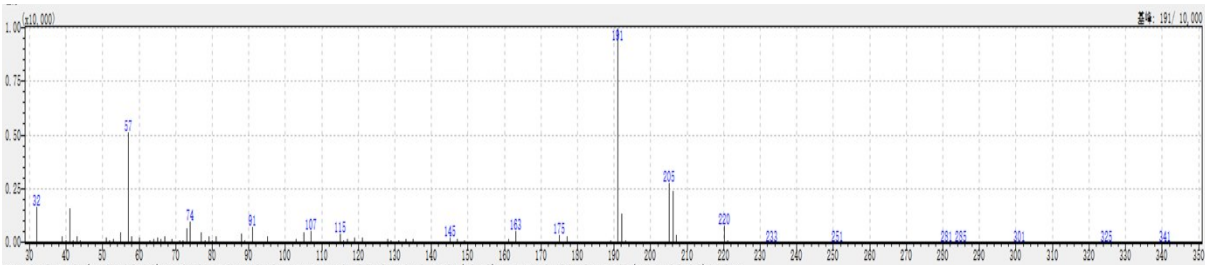

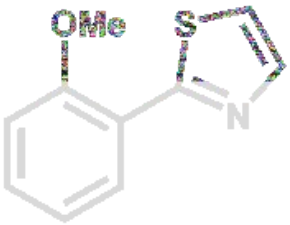

2-(2-methoxyphenyl)thiazole: ^{1}H NMR (600 MHz, $CDCl_3$) δ 4.04 (s, 3H), 7.03-7.13 (m, 2H), 7.37-7.43 (m, 1H), 7.40 (d, *J* = 3.3 Hz, 1H), 7.92 (d, *J* = 3.3 Hz, 1H), 8.41 (m, 1H); MS calculated for $C_{10}H_9NOS$: 191, found: 191.

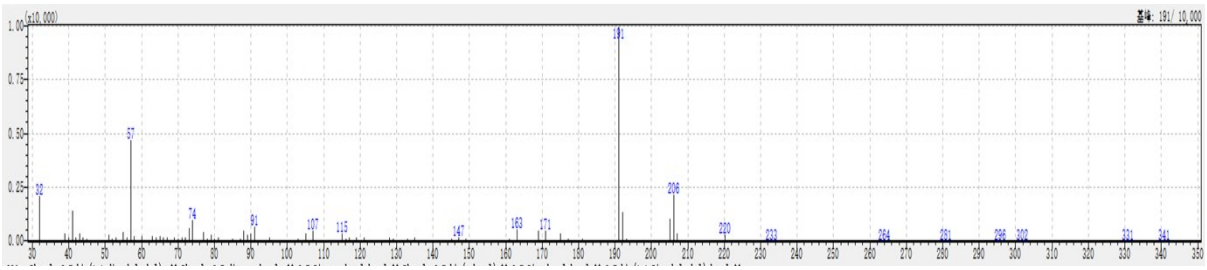

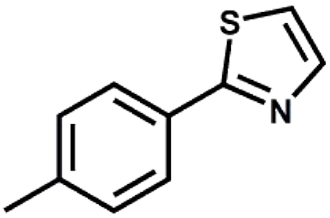

2-(4-Methylphenyl)thiazole： ^{1}H NMR (600 MHz, $CDCl_3$) δ 2.39 (s, 3H), 7.25 (d, *J* = 8.2 Hz, 2H), 7.29 (d, *J* = 3.5 Hz, 1H), 7.84 (d, *J* = 3.5 Hz, 1H), 7.88 (d, *J* = 8.2 Hz, 2H). MS calculated for $C_{10}H_9NS$: 175, found: 175.

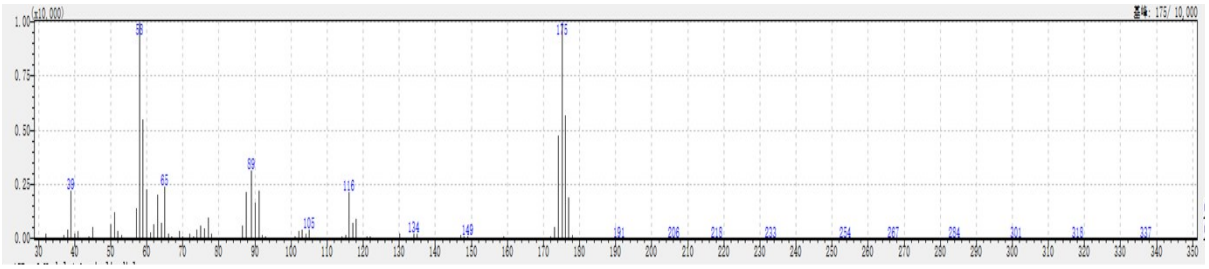

2-(3-Methylphenyl)thiazole： ^{1}H NMR (600 MHz, $CDCl_3$) δ 2.40 (s, 3H), 7.21 (d, *J* = 7.6 Hz, 1H), 7.27-7.33 (m, 2H), 7.74 (d, *J* = 8.0 Hz, 1H), 7.80 (s, 1H), 7.84 (d, *J* = 3.2 Hz, 1H). MS calculated for $C_{10}H_9NS$: 175, found: 175.

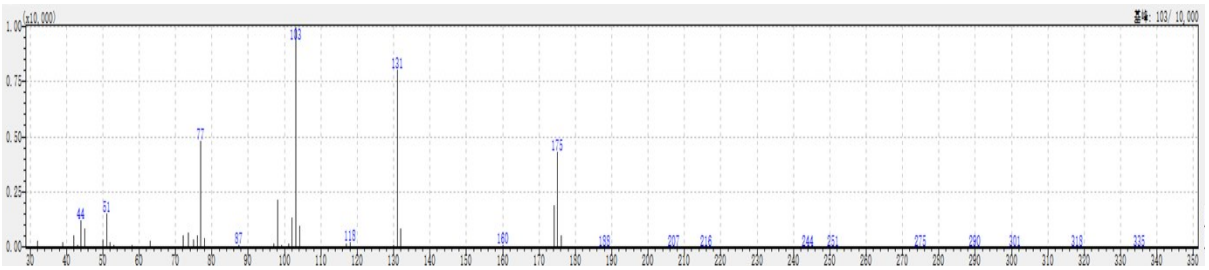

4-(Thiazol-2-yl)benzonitrile：^{1}H NMR (600 MHz, $CDCl_3$) δ 7.45 (d, *J* = 3.2 Hz, 1H) 7.74 (d, *J* = 8.8 Hz, 2H), 7.94 (d, *J* = 3.2 Hz, 1H), 8.09 (d, *J* = 8.4 Hz, 2H). MS calculated for $C_{10}H_6N_2S$: 186, found: 186.

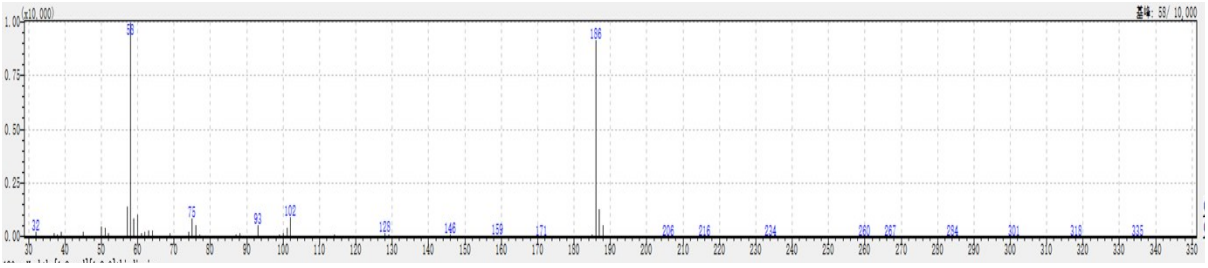

2-(4-Trifluoromethylphenyl)thiazole：^{1}H NMR (600 MHz, $CDCl_3$) δ 7.42 (d, *J* = 3.2 Hz, 1H), 7.70 (d, *J* = 8.2 Hz, 2H), 7.92 (d, *J* = 3.2 Hz, 1H), 8.08 (d, *J* = 8.2 Hz, 2H). MS calculated for $C_{10}H_6F_3NS$: 229, found: 229.

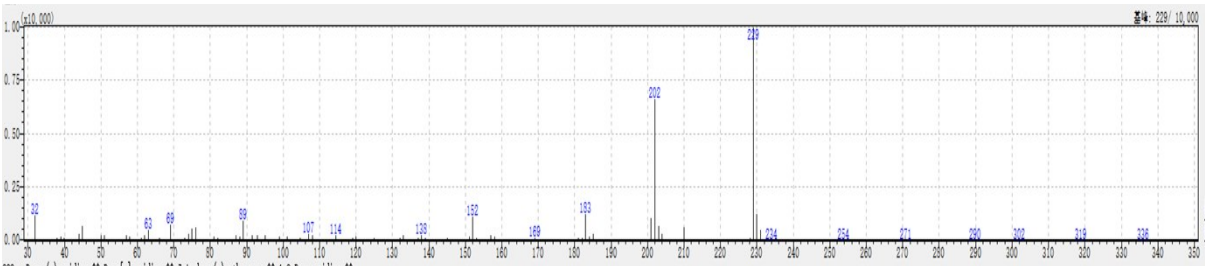

2-(4-Nitrophenyl)thiazole: ^{1}H NMR (600 MHz, $CDCl_3$) δ 7.47 (d, J = 3.5 Hz, 1H), 7.97 (d, J = 3.5 Hz, 1H), 8.12 (m, 2H), 8.29 (d, J = 8.2 Hz, 2H). MS calculated for $C_9H_6N_2O_2S$: 206, found: 206.

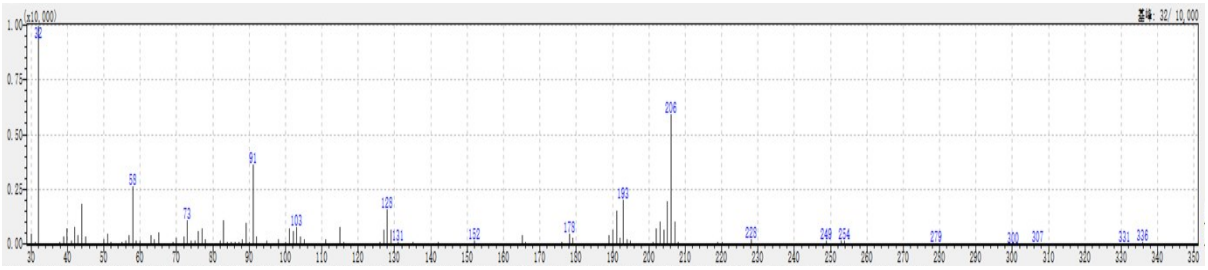

4-(Thiazol-2-yl)benzaldehyde: ^{1}H NMR (600 MHz, $CDCl_3$) δ 7.45 (d, J = 8.1 Hz, 1H), 7.95 (m, 3H), 8.17 (d, J = 8.2 Hz, 2H), 10.07 (s, 1H). MS calculated for $C_{10}H_7NOS$: 189, found: 189.

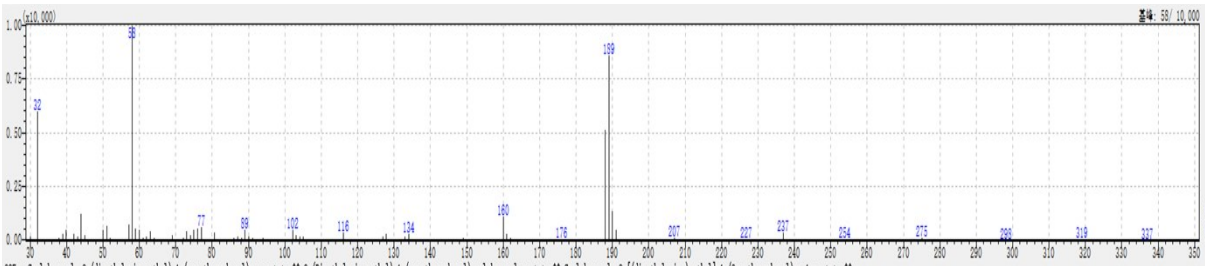

N-methyl-2-phenylimidazole: ^{1}H NMR (600 MHz, $CDCl_3$) δ 3.72 (s, 3H), 6.97 (s, 1H), 7.12 (s, 1H), 7.37-7.46 (m, 3H), 7.61 (d, *J* = 8.0 Hz, 2H). MS calculated for $C_{10}H_{10}N_2$: 158, found: 158.

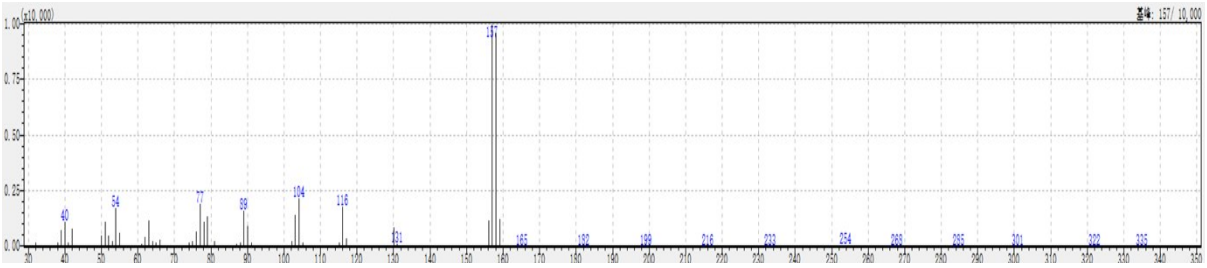

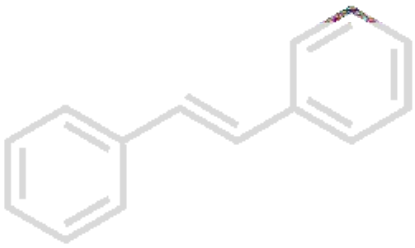

(E)-Stilbene: ^{1}H NMR (600 MHz, $CDCl_3$) δ 7.11 (s, 2H), 7.25 (m, 2H), 7.31-7.37 (m, 4H), 7.50 (d, *J* = 7.8 Hz, 4H). MS calculated for $C_{14}H_{12}$: 180, found: 180.

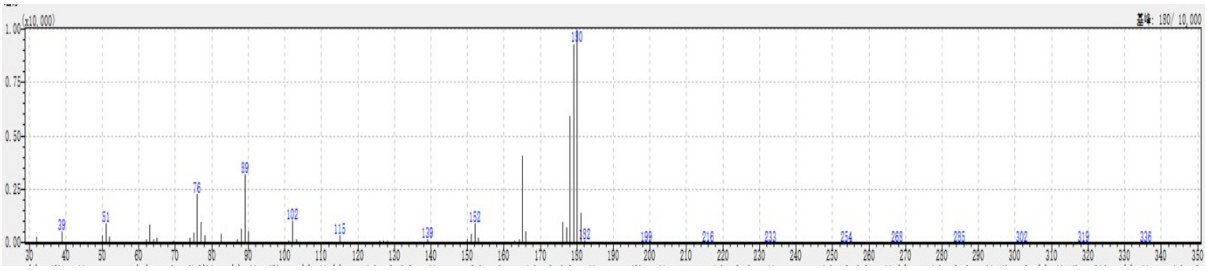

(E)-4-Methoxystilbene: ^{1}H NMR (600 MHz, $CDCl_3$) δ 3.83 (s, 3H), 6.90 (d, *J* = 8.6 Hz, 2H), 6.97 (d, *J* = 16.3 Hz, 1H), 7.09 (d, *J* = 16.3 Hz, 1H), 7.22 (m, 1H), 7.34 (m, 2H), 7.45 (d, *J* = 8.6 Hz, 2H), 7.51 (d, *J* = 7.6 Hz, 2H). MS calculated for $C_{15}H_{14}O$: 210, found: 210.

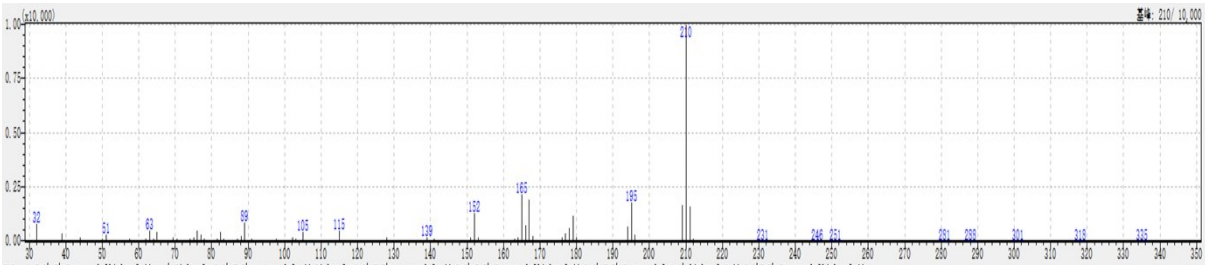

(E)-3-Methoxystilbene: ^{1}H NMR (600 MHz, $CDCl_3$) δ 3.88 (s, 3H), 6.87 (m, 1H), 7.10 (d, *J* = 2.6 Hz, 1H), 7.19-7.12 (m, 3H), 7.28-7.35 (m, 2H), 7.40 (m, 2H), 7.55 (m, 2H). MS calculated for $C_{15}H_{14}O$: 210, found: 210.

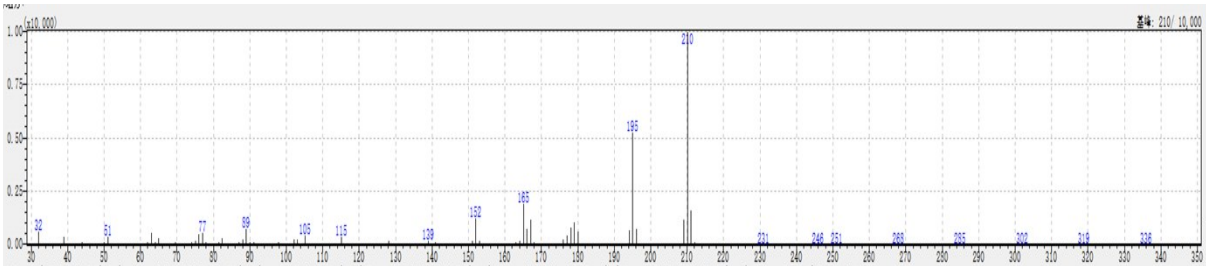

(E)-3-Methoxystilbene: ^{1}H NMR (600 MHz, $CDCl_3$) δ3.88 (s, 3H), 6.87 (m, 1H), 7.10 (m, 1H), 7.12-7.19 (m, 3H), 7.28-7.35 (m, 2H), 7.40 (m, 2H), 7.55 (m, 2H). MS calculated for $C_{15}H_{14}O$: 210, found: 210.

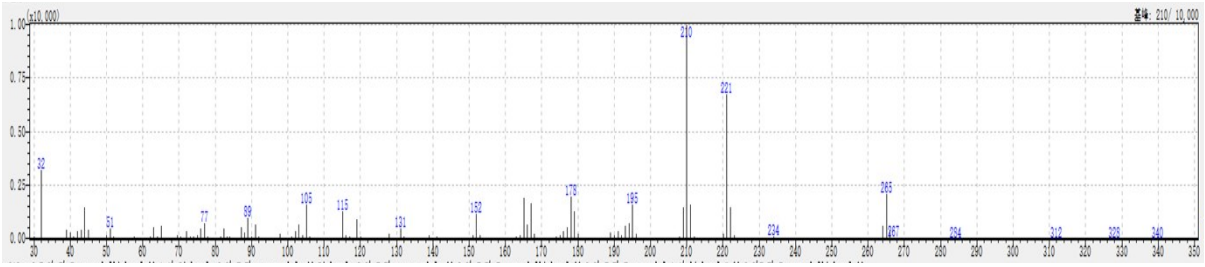

(E)-4-Methylstilbene: ^{1}H NMR (600 MHz, $CDCl_3$) δ 2.27 (s, 3H), 6.99 (m, 2H), 7.08 (d, *J*=8.0 Hz, 2H), 7.15 (m, 1H), 7.26 (m, 2H), 7.32 (d, *J*=8.0 Hz, 2H), 7.41 (d, *J*=7.2 Hz, 2H). MS calculated for $C_{15}H_{14}$: 194, found: 194.

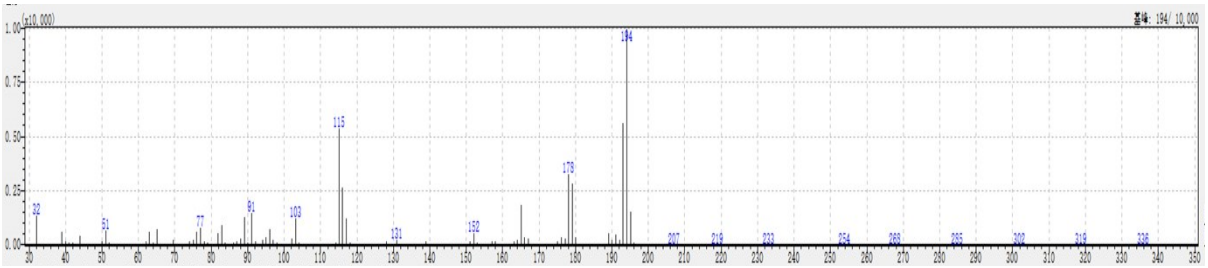

(E)-3-Methylstilbene: ^{1}H NMR (600 MHz, $CDCl_3$) δ 2.41 (s, 3H), 7.16-7.08 (m, 3H), 7.26-7.31 (m, 2H), 7.33-7.41 (m, 4H), 7.54 (m, 2H). MS calculated for $C_{15}H_{14}$: 194, found: 194.

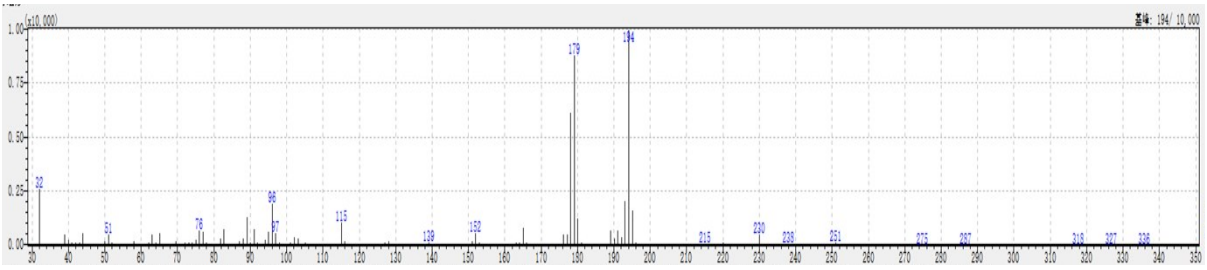

(E)-4-Nitrostilbene: ^{1}H NMR (600 MHz, $CDCl_3$) δ 7.07 (d, *J* = 16.4 Hz, 1H) 7.20 (d, *J*=16.2 Hz, 1H), 7.26 (m, 1H), 7.33 (m, 2H), 7.48 (d, *J* =7.2 Hz, 2H), 7.56 (d, *J*=8.8 Hz, 2H), 8.16 (d, *J*=8.8 Hz, 2H). MS calculated for $C_{14}H_{11}NO_2$: 225, found: 225.

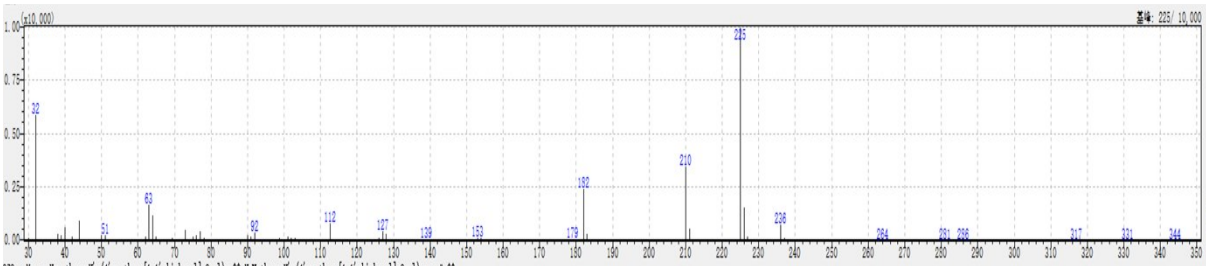

(E)-4-Cyanostilbene: ^{1}H NMR (600 MHz, $CDCl_3$) δ 6.97 (d, *J*=16.4 Hz, 1H), 7.09 (d, *J*=16.4 Hz, 1H), 7.21 (m, 1H), 7.28 (m, 2H), 7.41-7.48 (m, 4H), 7.51 (d, *J*=8.0 Hz, 2H). MS calculated for $C_{15}H_{11}N$: 205, found: 205.

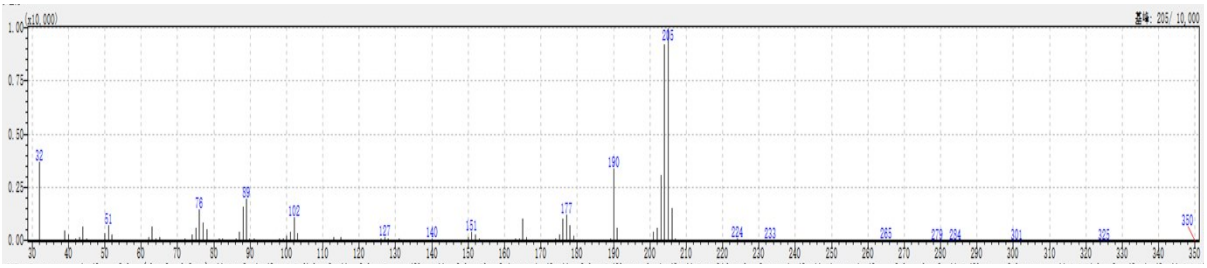

(E)-4-Trifluoromethylstilbene: ^{1}H NMR (600 MHz, $CDCl_3$) δ 7.02 (d, *J*=16.4 Hz, 1H), 7.10 (d, *J*=16.4 Hz, 1H), 7.21 (m, 1H), 7.29 (m, 2H), 7.44 (d, *J*=7.2 Hz, 2H), 7.51 (s, 4H). MS calculated for $C_{15}H_{11}F_3$: 248, found: 248.

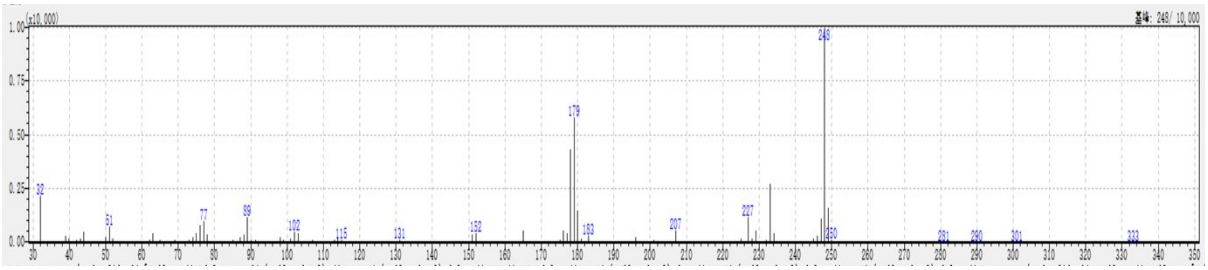

(E)-(2-cyclohexylvinyl)benzene: ^{1}H NMR (600 MHz, $CDCl_3$) δ 1.15-1.42 (m, 5H), 1.67-1.88 (m, 5H), 2.10-2.21 (m, 1H), 6.21 (m, 1H), 6.38 (m, 1H), 7.21 (t, *J* = 7.2 Hz, 1H), 7.31 (m, 2H),7.35-7.40 (m, 2H). MS calculated for $C_{14}H_{18}$: 186, found: 186.

Benzophenone: ^{1}H NMR (600 MHz, $CDCl_3$) δ 7.47 (t, *J* = 7.6 Hz, 4H), 7.57 (d, *J* = 7.2 Hz, 2H), 7.79-7.81 (m, 4H). MS calculated for $C_{15}H_{11}F_3$: 182, found: 182.

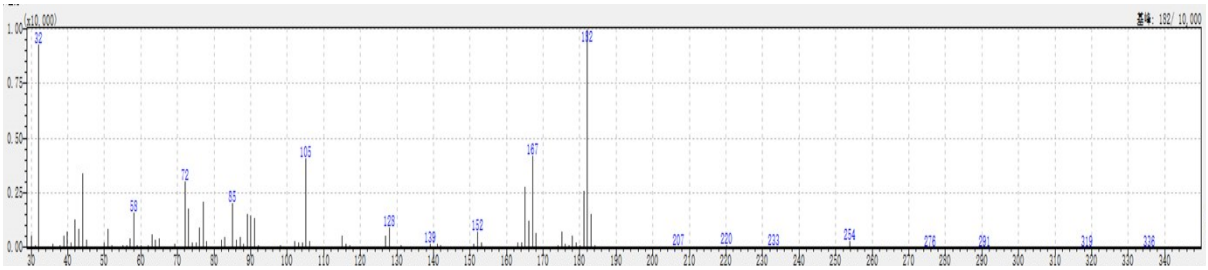

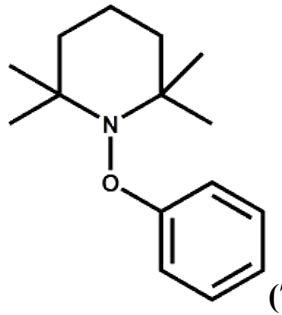

(7)

TEMPO-benzene 7, MS calculated for $C_{15}H_{23}NO$: 233, found: 233

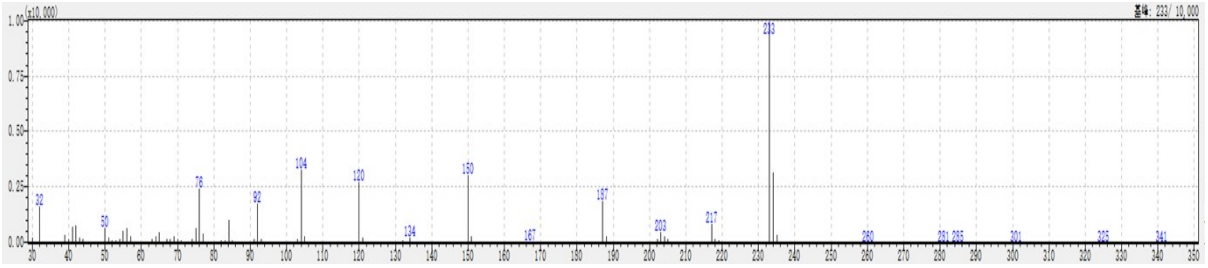

(9aa)

2-Phenylacetophenone 9aa: MS calculated for $C_{14}H_{12}O$: 196, found: 196.

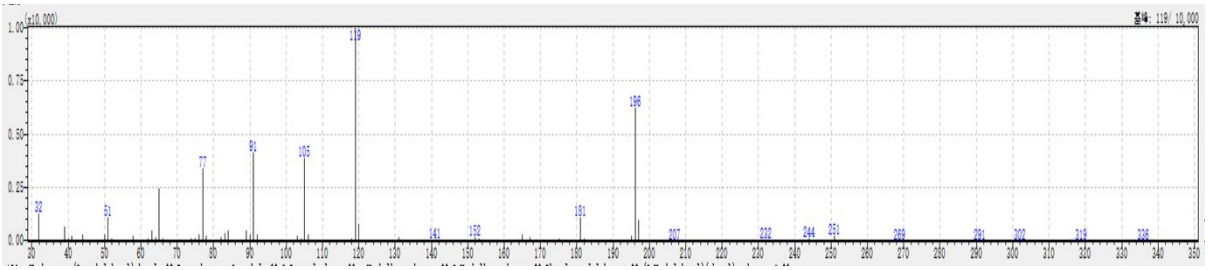

References

[S1] P. Horcajada, C. Serre, G. Maurin, N.A. Ramsahye, F. Balas, M. Vallet-Regí, M. Sebban, F. Taulelle, G. Férey; *J. Am. Chem. Soc.* 2008, **130**, 6774-6780.

[S2] D.K. Wang, R.K. Huang, W.J. Liu, D.G. Sun, Z.H. Li; *ACS Catal.*, 2014, **4**, 4254-4260.

[S3] D.K. Wang, M.T. Wang, Z.H. Li; *ACS Catal.* 2015, **5**, 6852-6857.

[S4] Q.L. Zhu, J. Li, Q. Xu; *J. Am. Chem. Soc.* 2013, **135**, 10210-10213.

[S5] D.K. Wang, Z.H. Li; *J. Catal.* 2016, **342**, 151-157.

[S6] P. Horcajada, S. Surble, C. Serre, D.Y. Hong, Y.K. Seo, J.S. Chang, J.M. Greneche, I. Margiolaki, G. Ferey; *Chem. Commun.* 2007, **27**, 2820-2822.

[S7] W.F. Dong, X.D. Liu, W.B. Shi, Y.M. Huang; *RSC Adv.* 2015, **5**, 17451-17457.

[S8] G. Férey, C. Mellot-Draznieks, C. Serre, F. Millange, J. Dutour, S. Surblé, I. Margiolaki; *Science.* 2005, **309**, 2040-2042.

[S9] G.Q. Song, Z.Q. Wang, L. Wang, G.R. Li, M.J. Huang, F.X. Yin; *Chin. J. Catal.* 2014, **35**, 185-195.

[S10] D.Y. Yu, M.H. Wu, Q. Hu, L.L. Wang, C.C. Lv, L. Zhang; *J. Hazard. Mater,* 2019, **367**, 456-464.

[S11] L.H. Ai, L.L. Li, C.H. Zhang, J. Fu, J. Jiang; *Chem. Eur. J.* 2013, **19**, 15105-15108.

[S12] F.C. Tan, M.L. Liu, K.Y. Li, Y.R. Wang, J.H. Wang, X.W. Guo, G.L. Zhang, C.S. Song; *Chem. Eng. J.* 2015, **281**, 360-367.

[S13] C. Gao, S. Chen, X. Quan, H.T. Yu, Y.B. Zhang; *J. Catal.* 2017, **356**, 125-132.

[S14] W.X. Guo, W.W. Sun, L.P. Lv, S.F. Kong, Y. Wang; *ACS Nano*. 2017, **11**, 4198-4205.

[S15] D.D. Martins, H.M. Alvarez, L.C.S. Aguiar, O.A.C. Antunes; *Appl. Catal A-Gen.* 2010, **408**, 47-53.

[S16] J. Ji, P. Liu, P.P. Sun; *Chem. Commun.* 2015, **51**, 7546-7549.